

Uplink Rate-Splitting Multiple Access for Mobile Edge Computing with Short-Packet Communications

Jiawei Xu, Yumeng Zhang, Yunnuo Xu, Bruno Clerckx, *Fellow, IEEE*

Abstract—In this paper, a Rate-Splitting Multiple Access (RSMA) scheme is proposed to assist a Mobile Edge Computing (MEC) system where local computation tasks from two users are offloaded to the MEC server, facilitated by uplink RSMA for processing. The efficiency of the MEC service is hence primarily influenced by the RSMA-aided task offloading phase and the subsequent task computation phase, where reliable and low-latency communication is required. For this practical consideration, short-packet communication in the Finite Blocklength (FBL) regime is introduced. In this context, we propose a novel uplink RSMA-aided MEC framework and derive the overall Successful Computation Probability (SCP) with FBL consideration. To maximize the SCP of our proposed RSMA-aided MEC, we strategically optimize: (1) the task offloading factor which determines the number of tasks to be offloaded and processed by the MEC server; (2) the transmit power allocation between different RSMA streams; and (3) the task-splitting factor which decides how many tasks are allocated to splitting streams, while adhering to FBL constraints. To address the strong coupling between these variables in the SCP expression, we apply the Alternative Optimization method, which formulates tractable subproblems to optimize each variable iteratively. The resultant non-convex subproblems are then tackled by Successive Convex Approximation. Numerical results demonstrate that applying uplink RSMA in the MEC system with FBL constraints can not only improve the SCP performance but also provide lower latency in comparison to conventional transmission scheme such as Non-orthogonal Multiple Access (NOMA).

Index Terms—Rate-Splitting Multiple Access (RSMA), Non-orthogonal Multiple Access (NOMA), Mobile Edge Computing (MEC), Successful Computation Probability (SCP).

I. INTRODUCTION

It is envisioned that 6th Generation (6G) will enable ubiquitous connectivity for a massive number of devices and provide low-latency and high-reliability communications services, such as the tactile Internet, remote surgery, and autonomous driving [1], [2]. These computation-intensive and latency-sensitive applications challenge both the computational capabilities of User Equipments (UEs) and the processing efficiency of Mobile Cloud Computing (MCC). A significant bottleneck for MCC lies in the long propagation distances between end

users and remote cloud centers, resulting in substantial latency for mobile applications. It is widely acknowledged that relying only on Cloud Computing is insufficient to achieve the millisecond-level latency targets required for computing and communication in 6G networks [3]. Additionally, the massive data exchange between end users and remote cloud servers risks overwhelming and congesting networks, potentially leading to network bottlenecks. In contrast to MCC, Mobile Edge Computing (MEC) allows UEs to offload their workloads to edge servers for nearby processing, improving computing performance and lowering network latency [4], [5].

The concept of MEC was firstly proposed by the European Telecommunications Standard Institute (ETSI) in 2014, and was defined as a new platform providing IT and cloud computing capabilities within the Radio Access Networks (RAN) in close distance to mobile subscribers [6]. The definition of MEC is based on offloading computation-intensive tasks from UEs to an edge device named MEC server which provides computing services to multiple UEs. Offloading data from a large number of UEs to MEC servers substantially exacerbates the issue of spectrum scarcity. Therefore, in order to achieve high spectral efficiency, energy efficiency and guarantee the Quality of Service (QoS) of MEC networks, wireless resources must be used effectively and appropriate multiple access techniques are needed. [7]–[9] have investigated the resource allocation problem in Time Division Multiple Access (TDMA), Frequency Division Multiple Access (FDMA) and Orthogonal Frequency Division Multiple Access (OFDMA) aided-MEC systems, respectively, demonstrating the benefit of offloading. Compared to these Orthogonal Multiple Access (OMA) schemes, Non-orthogonal Multiple Access (NOMA) has been recognized as an enabler to improve both the spectral and energy efficiency [10]–[13].

NOMA has been widely investigated and applied in the MEC network to improve energy efficiency, reliability and/or latency [14]–[20]. The authors combined NOMA and MEC in [14]–[16] to optimize the weighted sum-energy consumption with the constraints of computation latency. Offloading delay minimization problem of NOMA-MEC network has been investigated in [17], [18], where [17] derived closed-form expressions for the optimal task partition ratio and offloading transmit power, [18] has proposed and compared two algorithms to solve the optimization problem and further established the

J. Xu is with Imperial College London. B. Clerckx is with the Department of Electrical and Electronic Engineering at Imperial College London, London SW7 2AZ, UK. (email: j.xu20,b.clerckx@imperial.ac.uk). Yumeng Zhang is with the Department of Electronics and Computer Engineering, The Hong Kong University of Science and Technology, Hong Kong 999077, China (e-mail: eeyzhang@ust.hk). Yunnuo Xu is with the School of Information Science and Engineering, Shandong University, Qingdao 266237, China (e-mail: yunnuo.xu@sdu.edu.cn).

criteria to select the working modes of MEC offloading. As Successful Computation Probability (SCP) which refers to the probability that a computation-intensive task is successfully completed, considering constraints such as latency and resources, is an important metric in an MEC system, an SCP maximization problem has been formulated and closed-form expressions for SCP have been derived in [19], demonstrating the gain of NOMA over OMA. The overall error probability of NOMA-aided MEC network with the consideration of imperfect Successive Interference Cancellation (SIC) has been studied in [20]. The numerical results have shown the performance improved with the implementation of NOMA, however, multi-antenna NOMA can impose heavy computational burdens on the transmitters and the receivers. Besides, it can also be sensitive to the user deployment. These disadvantages make NOMA not suitable for 6G MEC network [21].

In recent years, Rate-Splitting Multiple Access (RSMA), relying on linearly precoded rate-splitting at the transmitter and SIC at the receiver, has emerged as a promising multiple access technique for 6G. By splitting user messages, RSMA can softly bridge NOMA and Space Division Multiple Access (SDMA) [22]–[25]. Downlink and uplink RSMA have been demonstrated the capability of offering significant gains in terms of energy efficiency, user fairness, and latency reduction [22], [23], [26]–[28] in both Finite Blocklength (FBL) and Infinite Blocklength (IFBL). There have been a few works investigating the application of RSMA in MEC network [29]–[31]. The downlink RSMA principles have been utilized to facilitate the offloading of users' computation tasks to multiple MEC servers concurrently [29]. A hybrid RSMA-TDMA scheme for an MEC system has been proposed to minimize delay [30]. The sum of users' maximum delay has been minimized through jointly optimizing computation task assignment ratios, transmission power and computational resources. Instead of investigating delay minimization, the authors in [31] have utilized RSMA in assisting MEC system to achieve the maximum achievable rate of secondary users while maintaining the performance of primary users. Besides, the authors have formulated an SCP maximization problem and derived the closed-form expressions for SCP. With the aid of RSMA, the performance of MEC network has been enhanced compared to NOMA-aided MEC system [19].

Although MEC has been widely investigated in terms of radio-and-computational resource allocation to improve the latency performance, aforementioned studies are based on conventional Shannon capacity, which is based on the assumption of an arbitrarily low decoding error probability with IFBL, and it is no longer applicable to latency-critical systems. Because IFBL does not fully reflect the real-world situation, where wireless communications are always subject to a certain reliability, and the transmission rate and the time slots allocation can impact the error probability of transmission [32]. Polyanskiy et al. have provided information-theoretic limits on the achievable rate for given FBL and error probability in Additive White Gaussian Noise (AWGN) channels [33]. Then the maximum channel coding rate has

TABLE I
COMPARISON OF THIS PAPER TO THE PREVIOUS WORKS.

Reference	NOMA	RSMA	SCP	FBL
[7]–[9]	×	×	×	×
[17], [18], [20]	✓	×	×	×
[19]	✓	×	✓	×
[29], [30]	×	✓	×	×
[31]	✓	✓	✓	×
[42]	✓	×	×	✓
[20], [43], [44]	✓	×	✓	✓
This work	✓	✓	✓	✓

been extended to quasi-static fading channels in [34]–[36] as well as in QoS-constraint network in [37] with constraints on error probability, blocklength and long-term transmit power for point-to-point communication scenarios. The maximum achievable transmission rate has been studied for quasi-static Multiple-Input Multiple-Output (MIMO) fading channels in [38] under both Channel State Information at Transmitter (CSIT)/Channel State Information at Receiver (CSIR) settings for a single user. To capture the impact of interference from multi-users within FBL coding, [39]–[41] have examined the achievable coding rate with a scenario involving K users.

According to the latency-critical requirement of MEC, investigating MEC in FBL regime becomes necessary. Some research has been carried out on MEC in FBL regime [20], [42]–[44] in terms of energy efficiency, reliability, and latency, respectively. However, all those works are based on TDMA or NOMA transmission schemes. The differences and comparisons between this work and previous works are listed in Table I. Motivated by 1) the need of state-of-art of multiple access in MEC network, 2) the appealing performance of RSMA, and 3) to capture the crucial feature of latency-critical requirements of MEC, we propose an uplink RSMA-assisted MEC framework and investigate its performance with the constraint of FBL in terms of reliability and latency. The contributions of this work are summarized as follows.

A. Contributions

- First, for the *first time*, uplink RSMA with short-packet communications is introduced into MEC system as a powerful multiple access to facilitate with the uplink task offloading procedure. The practical study of offloading task data with finite blocklength is noteworthy since it is an essential aspect for low-latency applications in 6G and future wireless networks.
- Second, the SCP performance of RSMA-aided MEC under FBL constraints is analyzed. This work aims to maximize SCP performance by optimizing the entire system strategy with FBL considerations, including the offloading factor, representing the number of tasks to be processed by the MEC server, the task-splitting factor, representing the number of offloading tasks assigned to each stream in the RSMA scheme and the power allocated to each splitting stream. A

closed-form expression of the offloading factor is derived. Due to the coupling among the remaining optimization variables, Alternative Optimization (AO) is applied to decompose the original problem into several sub-problems, each addressed by the proposed Successive Convex Approximation (SCA)-based method. This is the first work to offer a comprehensive optimization of systemic parameters for RSMA-aided MEC systems with FBL constraints.

- Through simulations, the performance of RSMA-aided MEC system is analyzed. Simulation results show that splitting messages of RSMA helps in MEC deployments because of the flexibility of the decoding order to balance the Signal to Interference plus Noise Ratio (SINR) between each stream. Moreover, RSMA can achieve a higher SCP than NOMA with a shorter blocklength, thereby reducing the latency. Besides, the performance gain of RSMA over NOMA in the FBL regime saturates as the blocklength becomes sufficiently large. Numerical results demonstrate RSMA-aided MEC achieves more reliable communication in FBL regime with higher SCP compared to NOMA.

B. Organization

The rest of the paper is organized as follows. The system model of the RSMA-aided MEC in with FBL is specified in Section II. The SCP is defined and derived in Section III. The problem is formulated and optimized in Section IV. Simulation results are presented in Section V and we conclude the paper in Section VI.

C. Notations

Italic and bold lower-case denote scalars and vectors, respectively. $|\cdot|$ denotes the absolute value if the argument is a scalar or the cardinality if the argument is a set. $\cdot \setminus \cdot$ denotes the difference between two sets if the arguments are sets. $\mathcal{CN}(\mu, \sigma^2)$ denotes circular symmetric complex Gaussian distribution with mean μ and variance σ^2 .

II. SYSTEM MODEL

This section models an RSMA-aided Single-Input Single-Output (SISO) MEC system with two users, indexed by $\mathcal{K} = \{1, 2\}$. Due to the limited local computation capabilities of the two users, this section characterizes an MEC scheme that schedules both users to simultaneously offload their data to an MEC server with high computation capability. Facilitated by the MEC server, both users can accomplish their tasks within the time budget by downloading the results from the MEC server. Specifically, it is assumed that each user, with a computational capability of f_{user} Hz/cycle, needs to complete a computation task of M_k , $k \in \mathcal{K}$ bits within T s. In practice, the scenario often arises that $M_k C_{\text{cpu}} / f_{\text{user}} > T$, where C_{cpu} represents the number of required Central Processing Unit (CPU) cycles to compute one-bit task, necessitating the involvement of a central MEC server with a computational capability of

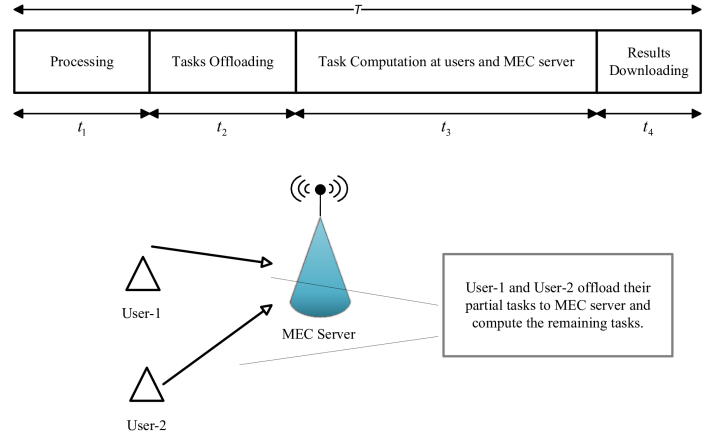


Fig. 1. The RSMA-aided MEC system with two users.

$f_{\text{MEC}} = L f_{\text{user}}$ ($L > 1$). Assume that the M_k -bits task at each user is bit-wise independent and can be arbitrarily divided into subtasks. Hence, to meet the time budget T , each user- k offloads a part of their task of $\lambda_k M_k$ bits, with λ_k , $0 \leq \lambda_k \leq 1$, being the offloading factor of user- k , to the MEC server with the assistance of uplink RSMA. The remaining tasks of $(1 - \lambda_k) M_k$ bits are executed locally to exploit users' own local computation capability. $\lambda_k = 0$ and $\lambda_k = 1$ represent the fully local computation and fully offloading computation, respectively.

The whole procedure of the RSMA-aided MEC system is shown in Fig. 1, which consists of four stages. In the first stage, the offloading factor, task-splitting factor and power allocation are determined for two users within the processing time t_1 s. The rate-splitting power allocation factors guarantee the bit error rate performance of RSMA in the offloading stage. Then, in the second stage, users offload their tasks to the MEC server by uplink RSMA transmission within time duration t_2 s. Thereafter, the third stage performs task execution at both the MEC server and the two local users within time duration t_3 s. We assume the MEC server starts to compute the tasks immediately after the offloading is finished, i.e., there is no queue delay at the MEC server. In the last stage, the computed results of the offloaded tasks are downloaded by users, which consumes time t_4 s. Compared to the offloading time t_2 and execution time t_3 , t_1 and t_4 can be ignored since the resultant data often features a very small size compared with the offloading data size in t_2 s [45]. Therefore, the time of offloading computation mainly comes from the time of tasks offloading stage t_2 and the time of tasks execution stage t_3 , i.e., in the following of this paper, we set the time constraint to be $t_2 + t_3 \leq T$ without loss of generality.

In the reminder of this section, we detail the involved tasks offloading phase (stage 2) in subsection II-A, and the execution parameters in tasks computation phase (stage 3) in subsection II-B, respectively. Upon this, we are able to formulate the successful offloading probability of stage 2, the successful execution probability of stage 3 and the successful computation probability in Section III.

A. Tasks Offloading Phase

In this subsection, the details of tasks offloading from two users to the MEC server are presented.

1) *RSMA*: The two-user SISO uplink RSMA with perfect CSIT and CSIR system is considered. In the two-user uplink RSMA, one user's task is split following the uplink RSMA principle. We assume user-1 split its task W_1 into two parts, $W_{1,d}$, $d \in \{1, 2\}$ and the task of user-2 stays unsplit. These three split tasks $W_{1,1}$, $W_{1,2}$, and W_2 then are encoded independently, resulting into three streams $s_{1,1}$, $s_{1,2}$ and s_2 , to be transmitted in total. The transmit power of user- k is denoted as P_k . The received signal at the MEC server is expressed as

$$y = h_1 \sqrt{P_{1,1}} s_{1,1} + h_1 \sqrt{P_{1,2}} s_{1,2} + h_2 \sqrt{P_2} s_2 + n, \quad (1)$$

where $P_{1,d}$, $d \in \{1, 2\}$ is the transmit power of stream $s_{1,d}$ and $\sum_{d=1}^2 P_{1,d} \leq P_1$. $n \sim \mathcal{CN}(0, \sigma_n^2)$ is the complex AWGN at the MEC server.

At the MEC server, SIC is applied to decode three streams and all possible decoding orders can be classified into three cases, i.e., (i) $s_{1,1} \rightarrow s_2 \rightarrow s_{1,2}$ (i.e. the MEC server decodes $s_{1,1}$ first, followed by s_2 , and finally $s_{1,2}$), (ii) $s_{1,1} \rightarrow s_{1,2} \rightarrow s_2$ and (iii) $s_2 \rightarrow s_{1,1} \rightarrow s_{1,2}$.¹ By utilizing chain rule, the achievable rates of user-1 and user-2 obtained by employing the decoding order (ii) and (iii) are equal to those obtained by employing the decoding order $s_1 \rightarrow s_2$ and $s_2 \rightarrow s_1$ of NOMA, respectively. Besides, based on the previous study [26], uplink RSMA with the decoding order (i) can provide a much lower error probability compared to NOMA in short-packet communication. Therefore, the decoding order $s_{1,1} \rightarrow s_2 \rightarrow s_{1,2}$ is adopted in the following demonstration.

Since $s_{1,1}$ is decoded first by treating other signals as noise, the SINR $\gamma_{1,1}$ of $s_{1,1}$ is

$$\gamma_{1,1} = \frac{P_{1,1}|h_1|^2}{P_{1,2}|h_1|^2 + P_2|h_2|^2 + \sigma_n^2}. \quad (2)$$

Assuming $s_{1,1}$ is successfully decoded, its reconstructed task $\hat{W}_{1,1}$ is subtracted from the original received signal y to obtain y' . Then, the SINR of the second decoded stream s_2 expresses as

$$\gamma_2 = \frac{P_2|h_2|^2}{P_{1,2}|h_1|^2 + \sigma_n^2}. \quad (3)$$

Once $s_{1,2}$ is successfully decoded, its reconstruction $\hat{W}_{1,1}$ is subtracted from the received signal y' . Thus, the SINR of the last decoded stream $s_{1,2}$ is

$$\gamma_{1,2} = \frac{P_{1,2}|h_1|^2}{\sigma_n^2}. \quad (4)$$

Finally, if $s_{1,2}$ is successfully decoded, the estimated task \hat{W}_1 for user-1 is obtained by combining $\hat{W}_{1,1}$ and $\hat{W}_{1,2}$.

The data size of offloading tasks from three transmitted streams is defined as $M_{1,1} = \beta \lambda_1 M_1$, $M_2 = \lambda_2 M_2$ and

$M_{1,2} = (1 - \beta) \lambda_1 M_1$, where β is the task-splitting factor satisfying $0 \leq \beta \leq 1$. Then, the total received tasks data size at the MEC server is given as

$$M_{\text{MEC}} = \lambda_1 M_1 + \lambda_2 M_2. \quad (5)$$

Therefore, the Shannon capacity for each stream can be expressed as

$$\begin{aligned} C(\gamma_{1,1}) &= \log_2(1 + \gamma_{1,1}), \\ C(\gamma_2) &= \log_2(1 + \gamma_2), \\ C(\gamma_{1,2}) &= \log_2(1 + \gamma_{1,2}). \end{aligned} \quad (6)$$

Due to the consideration of uplink RSMA with FBL, the total transmission time for offloading is

$$t_2 = NT_s, \quad (7)$$

where N is the blocklength (in symbol) and T_s is the symbol duration. We assume the blocklength N for each stream is the same.

2) *NOMA*: NOMA is a particular instance of the system model of Section II-A1, since $0 \leq P_{1,1} \leq P_1$, we can regard NOMA as a subset of RSMA. The tasks W_1 and W_2 from user-1 and user-2 are encoded into s_1 and s_2 , respectively. The received signal at the MEC server is expressed as $y = h_1 \sqrt{P_1} s_1 + h_2 \sqrt{P_2} s_2 + n$.

Remark 1: If $P_{1,1}$ in RSMA scheme is set to P_1 or 0, RSMA boils down to NOMA with decoding order of $s_1 \rightarrow s_2$ or $s_2 \rightarrow s_1$, respectively. Since $0 \leq P_{1,1} \leq P_1$, we can regard NOMA as a subset of RSMA.

B. Tasks Computation Phase

In this subsection, we discuss the details of the hybrid computations, including local computation at the users and offloading computation at the MEC server, respectively.

For the local computation at user- k , the data size of the tasks is $(1 - \lambda_k)M_k$, and the required computation time at user- k is

$$t_3^k = \frac{(1 - \lambda_k)M_k C_{\text{cpu}}}{f_{\text{user}}}, \quad \forall k \in \mathcal{K}, \quad (8)$$

where C_{cpu} represents the number of CPU cycles required for one-bit task computing. f_{user} denotes the computation capabilities of users and we assume the capacity of each user is the same.

For offloading computation at the MEC server, we assume the computation capability of the MEC server $f_{\text{MEC}} = Lf_{\text{user}}$ with $L > 1$ to indicate the difference between users' and MEC server's computational capabilities. Thus, the required computation time at the MEC server is

$$t_3^{\text{MEC}} = \frac{M_{\text{MEC}} C_{\text{cpu}}}{f_{\text{MEC}}} = \frac{M_{\text{MEC}} C_{\text{cpu}}}{L f_{\text{user}}}. \quad (9)$$

Thus, the time duration t_3 for tasks computation is expressed as

$$\begin{aligned} t_3 &= \max\{t_3^k, t_3^{\text{MEC}}, \forall k \in \mathcal{K}\} \\ &= \max\left\{\frac{(1 - \lambda_k)M_k C_{\text{cpu}}}{f_{\text{user}}}, \frac{M_{\text{MEC}} C_{\text{cpu}}}{L f_{\text{user}}}, \forall k \in \mathcal{K}\right\}. \end{aligned} \quad (10)$$

¹By exchanging the orders of $s_{1,1}$ and $s_{1,2}$, the other three decoding orders are ignored in this letter without loss of generality.

III. SUCCESSFUL COMPUTATION PROBABILITY ANALYSIS

In this section, the SCP of RSMA-aided-MEC system with FBL is characterized. The SCP, denoted by P_s , is defined as the probability of the case that all tasks (including offloaded tasks to be computed at the MEC server and the remaining tasks to be computed by the users) are computed successfully within the delay budget T . Thus P_s contains two parts – the successful offloading probability, P_s^o , and the successful execution probability, P_s^e .

A. Successful Offloading Probability

The Shannon capacity definition states that under the assumption of IFBL, any rates inside the capacity region can be attained with an arbitrarily small error probability. However, in the case of an FBL regime, there are chances that rates inside the capacity region cannot be obtained with an arbitrarily small error probability. Therefore, the maximal achievable rate expression for FBL with a given error probability ϵ , is given by [33]

$$r \approx C(\gamma) - \sqrt{\frac{V(\gamma)}{N}} Q^{-1}(\epsilon), \quad (11)$$

where $C(\gamma)$ is the Shannon capacity calculated by (6) and $V(\gamma) = \left(1 - (1 + \gamma)^{-2}\right)$ is the channel dispersion. N is the blocklength, and Q is the Q-function². The error probability for a given data size M can be derived based on (11) as

$$\epsilon = Q\left(\frac{\log_2(1 + \gamma) - \frac{M}{N}}{\sqrt{V(\gamma)/N}}\right) = Q(f(\gamma, M)). \quad (12)$$

For uplink RSMA, we can write the error probability for each event listed above as: a) $s_{1,1}$ is incorrectly decoded; b) $s_{1,1}$ is correctly decoded but s_2 is incorrectly decoded; c) $s_{1,1}$ and s_2 are both correctly decoded but $s_{1,2}$ is incorrectly decoded. The error probability of every event can be expressed as

$$\begin{aligned} \epsilon_a &= Q(f(\gamma_a, M_a)), \\ \epsilon_b &= Q(f(\gamma_b, M_b)), \\ \epsilon_c &= Q(f(\gamma_c, M_c)), \end{aligned} \quad (13)$$

where $\gamma_a = \gamma_{1,1}$, $\gamma_b = \gamma_2$ and $\gamma_c = \gamma_{1,2}$. To simplify the analysis in the following Sec. IV, we change the subscript of M_k and β_k , $k \in \mathcal{K}$ to align with the subscript notation of three splitting streams. Specifically, the parameter M_i , $i \in \{a, b, c\}$, represents the data size of tasks transmitted by each stream which are $M_a = \beta_a \lambda_1 M_1$, $M_b = \beta_b \lambda_2 M_2$ and $M_c = \beta_c \lambda_1 M_1$, respectively. The parameter β_i , $i \in \{a, b, c\}$, represents the task-splitting factor between splitting streams where $\beta_a = \beta$, $\beta_b = 1$, and $\beta_c = 1 - \beta$. Then, the error probability of each user can be calculated as

$$\begin{aligned} \epsilon_1 &= \epsilon_a + (1 - \epsilon_a)\epsilon_b + (1 - \epsilon_a)(1 - \epsilon_b)\epsilon_c \\ &\approx \epsilon_a + \epsilon_b + \epsilon_c, \\ \epsilon_2 &= \epsilon_a + (1 - \epsilon_a)\epsilon_b \approx \epsilon_a + \epsilon_b. \end{aligned} \quad (14)$$

²Q-function is the tail distribution function of the standard normal distribution. Normally, Q-function is defined as: $Q(x) = \frac{1}{\sqrt{2\pi}} \int_x^\infty e^{-\frac{u^2}{2}} du$.

All the multiplied terms, e.g. $\epsilon_a \epsilon_b$ in (14) are ignored because the value is negligible. Therefore, the successful offloading probability P_s^o is given by

$$P_s^o = (1 - \epsilon_1)(1 - \epsilon_2). \quad (15)$$

B. Successful Execution Probability

As mentioned in Sec. II-A, the transmission time for offloading is calculated as $t_2 = NT_s$. When $t_3 \leq T - t_2$, the successful execution probability is $P_s^e = 1$. Otherwise, $P_s^e = 0$ if $t_3 \geq T - t_2$. Hence, we have $P_s^e = \mathbb{1}(t_3 \leq T - t_2)$. Therefore, the successful computation probability P_s can be written as

$$P_s = P_s^o P_s^e = \begin{cases} P_s^o, & t_3 \leq T - t_2 \\ 0, & t_3 \geq T - t_2 \end{cases} \quad (16)$$

Remark 2: If $\frac{M_k C_{\text{cpu}}}{f_{\text{user}}} \leq T$, both users can finish their tasks locally within the delay budget so offloading is not needed and we have $P_s = 1$.

IV. PROBLEM FORMULATION AND ALGORITHM

In this section, we aim to maximize the successful computation probability P_s by optimizing the rate-splitting power allocation for splitting user, $P_{1,1}$, $P_{1,2}$, the offloading factor, λ_i , $i \in \{a, b, c\}$, and task-splitting factor, β_i , $i \in \{a, b, c\}$, after which offloading is performed. Thus, the problem is formulated as

$$\max_{\mathbf{m}, \boldsymbol{\lambda}, \boldsymbol{\beta}} P_s \quad (17a)$$

$$\text{s.t. } P_{1,1} + P_{1,2} \leq P_t, \quad (17b)$$

$$P_2 \leq P_t, \quad (17c)$$

$$0 \leq \beta_i \leq 1, \quad i \in \{a, b, c\} \quad (17d)$$

$$t_2 + t_3 \leq T, \quad (17e)$$

where $\mathbf{m} = [P_{1,1}, P_{1,2}, P_2]^T$ represents the transmit power of each stream, $\boldsymbol{\lambda} = [\lambda_1, \lambda_2]^T$ denotes the offloading factor of each user and $\boldsymbol{\beta} = [\beta_a, \beta_b, \beta_c]^T$ denotes task-splitting factor between the splitting streams. From (15) and (16), we know that

$$\begin{aligned} P_s &= (1 - \epsilon_1)(1 - \epsilon_2) \\ &\approx 1 - \epsilon_1 - \epsilon_2 \\ &\approx 1 - (2\epsilon_a + 2\epsilon_b + \epsilon_c). \end{aligned} \quad (18)$$

Thus, Problem (17) is transformed into

$$\min_{\mathbf{m}, \boldsymbol{\lambda}, \boldsymbol{\beta}} 2\epsilon_a + 2\epsilon_b + \epsilon_c \quad (19a)$$

$$\text{s.t. } (17b), (17c), (17d), (17e).$$

According to the Chernoff bound of Q-function $\exp(-x^2/2) \geq Q(x)$, $x \geq 0.5$, we have

$$\exp\left(\frac{-f^2(\gamma_i, M_i)}{2}\right) \geq Q(f(\gamma_i, M_i)), \quad i \in \{a, b, c\}. \quad (20)$$

Therefore, we transform Problem (19) into Problem (21) to minimize the upper bound of the objective function.

$$\begin{aligned} \min_{\mathbf{m}, \boldsymbol{\lambda}, \boldsymbol{\beta}} \quad & 2 \exp\left(\frac{-f^2(\gamma_a, M_a)}{2}\right) + 2 \exp\left(\frac{-f^2(\gamma_b, M_b)}{2}\right) \\ & + \exp\left(\frac{-f^2(\gamma_c, M_c)}{2}\right) \\ \text{s.t.} \quad & (17\text{b}), (17\text{c}), (17\text{d}), (17\text{e}). \end{aligned} \quad (21\text{a})$$

Problem (21) is not convex and features strong coupling between variables in its objective function. For this kind of multi-variable-optimization problem, the classical AO algorithms have been widely applied to decompose the original problem into separate sub-problems to update each variable iteratively until convergence.

A. Offloading factor Optimization

In this subsection, we optimize $\boldsymbol{\lambda}$ under fixed power allocation factor, \mathbf{m} , and task-splitting factor, $\boldsymbol{\beta}$. The subproblem can be written as

$$\begin{aligned} \min_{\boldsymbol{\lambda}} \quad & 2 \exp\left(\frac{-f^2(\gamma_a, M_a)}{2}\right) + 2 \exp\left(\frac{-f^2(\gamma_b, M_b)}{2}\right) \\ & + \exp\left(\frac{-f^2(\gamma_c, M_c)}{2}\right) \\ \text{s.t.} \quad & t_3 \leq T - t_2. \end{aligned} \quad (22\text{a})$$

$$(22\text{b})$$

According to (7) and (10), constraint (22b) can be rewritten as

$$\frac{(1 - \lambda_k)M_k C_{\text{cpu}}}{f_{\text{user}}} \leq T - NT_s, \quad k \in \{1, 2\} \quad (23\text{a})$$

$$\frac{\sum_{k=1}^2 \lambda_k M_k C_{\text{cpu}}}{L f_{\text{user}}} \leq T - NT_s, \quad k \in \{1, 2\}. \quad (23\text{b})$$

Therefore, Problem (22) can be transformed into

$$\begin{aligned} \min_{\boldsymbol{\lambda}} \quad & 2 \exp\left(\frac{-f^2(\gamma_a, M_a)}{2}\right) + 2 \exp\left(\frac{-f^2(\gamma_b, M_b)}{2}\right) \\ & + \exp\left(\frac{-f^2(\gamma_c, M_c)}{2}\right) \\ \text{(23a), (23b).} \end{aligned} \quad (24\text{a})$$

Lemma 1: With fixed power allocation factor \mathbf{m} and task-splitting factor $\boldsymbol{\beta}$, the closed-form for λ_k is given by

$$\lambda_k^* = \max\left\{0, 1 - \frac{(T - NT_s)f_{\text{user}}}{M_k C_{\text{cpu}}}\right\}, \quad k \in \mathcal{K}. \quad (25)$$

Proof: For arbitrary \mathbf{m} and $\boldsymbol{\beta}$, the objective function $2 \exp\left(\frac{-f^2(\gamma_a, M_a)}{2}\right) + 2 \exp\left(\frac{-f^2(\gamma_b, M_b)}{2}\right) + \exp\left(\frac{-f^2(\gamma_c, M_c)}{2}\right)$ is clearly monotonically increasing with respect to (w.r.t) $\exp\left(\frac{-f^2(\gamma_i, M_i)}{2}\right)$, $i \in \{a, b, c\}$. Besides, each exponential function in the objective function is monotonically decreasing w.r.t $\lambda_k, k \in \mathcal{K}$. Therefore, the objective function in Problem (19) is monotonically increasing w.r.t λ_k (the proof of monotone is in Appendix 1). From constraint (23a), we can obtain the lower bound of λ_k

$$1 - \frac{(T - NT_s)f_{\text{user}}}{M_k C_{\text{cpu}}} \leq \lambda_k, \quad k \in \mathcal{K}. \quad (26)$$

If $1 - \frac{(T - NT_s)f_{\text{user}}}{M_k C_{\text{cpu}}} < 0$, then we have $T - NT_s > \frac{M_k C_{\text{cpu}}}{f_{\text{user}}}$, which means each user can finish its own tasks within the time budget and it is not necessary to offload task to MEC server. As the objective function is monotonically increasing, the optimal value of λ_k should be $\lambda_k^* = \max\{0, 1 - \frac{(T - NT_s)f_{\text{user}}}{M_k C_{\text{cpu}}}\}$, $k \in \mathcal{K}$.

B. Transmit Power Optimization

We now update \mathbf{m} following an AO structure. For fixed feasible task-splitting factor $\boldsymbol{\beta}$ and offloading factor $\boldsymbol{\lambda}$, we formulate the related subproblem by introducing slack variables $\mathbf{t} = [t_a, t_b, t_c]^T$ and $\boldsymbol{\rho} = [\rho_a, \rho_b, \rho_c]^T$ as follows

$$\min_{\mathbf{m}, \mathbf{t}, \boldsymbol{\rho}} \quad 2 \exp(-t_a) + 2 \exp(-t_b) + \exp(-t_c) \quad (27\text{a})$$

$$\text{s.t.} \quad t_i \leq \frac{N[\log(1 + \rho_i) - \frac{M_i}{N}]^2}{2[1 - (1 + \rho_i)^{-2}]}, \quad i \in \{a, b, c\} \quad (27\text{b})$$

$$\frac{P_{1,1}|h_1|^2}{P_{1,2}|h_1|^2 + P_2|h_2|^2 + \sigma_n^2} \geq \rho_a, \quad (27\text{c})$$

$$\frac{P_2|h_2|^2}{P_{1,2}|h_1|^2 + \sigma_n^2} \geq \rho_b, \quad (27\text{d})$$

$$\frac{P_{1,2}|h_1|^2}{\sigma_n^2} \geq \rho_c, \quad (27\text{e})$$

$$(17\text{b}), (17\text{c}).$$

In the following, we address each complex non-convex constraint in Problem (27) sequentially.

Constraint (27b) is intractable, and we first rewrite it into

$$\frac{t_i}{N}(1 - (1 + \rho_i)^{-2}) \leq \frac{1}{2} \left(\log(1 + \rho_i) - \frac{M_i}{N} \right)^2. \quad (28)$$

Since (28) is not convex, we first approximate the Right-Hand-Side (RHS) by its first-order Taylor expression, which is given by

$$\frac{1}{2} \left(\log(1 + \rho_i) - \frac{M_i}{N} \right)^2 \geq a_i^{[n]} \log(1 + \rho_i) + b_i^{[n]}, \quad (29)$$

where $a_i^{[n]} = \log(1 + \rho_i^{[n]}) - \frac{M_i}{N}$ and $b_i^{[n]} = \frac{1}{2}(a_i^{[n]})^2 - a_i^{[n]} \log(1 + \rho_i^{[n]})$.

Similarly, we introduce an additional auxiliary variable, $\mathbf{t}_1 = [t_{1,a}, t_{1,b}, t_{1,c}]$, to approximate the Left-Hand-Side (LHS) of constraint (28). Firstly, we rewrite LHS of (28) as follows

$$\frac{t_i}{N}(1 - (1 + \rho_i)^{-2}) = \frac{t_i}{N} - \frac{t_i(1 + \rho_i)^{-2}}{N}, \quad (30)$$

and we add the following constraints for the introduced variable:

$$t_{1,i} \leq t_i(1 + \rho_i)^{-2}. \quad (31)$$

Then (31) is transformed into

$$\log(t_{1,i}) + 2 \log(1 + \rho_i) \leq \log(t_i). \quad (32)$$

Since (32) is still not convex, $\log(t_{1,i})$ and $2\log(1 + \rho_i)$ are approximated by their first-order approximation around the point $(t_{1,i}^{[n]})$ and $(\rho_i^{[n]})$, which are given by

$$\log(t_{1,i}) \leq \log(t_{1,i}^{[n]}) + \frac{t_{1,i} - t_{1,i}^{[n]}}{t_{1,i}^{[n]}}, \quad (33a)$$

$$2\log(1 + \rho_i) \leq 2\log(1 + \rho_i^{[n]}) + \frac{2(\rho_i - \rho_i^{[n]})}{1 + \rho_i^{[n]}}. \quad (33b)$$

Then the constraint (28) can be rewritten into

$$\frac{t_1}{N} - \frac{t_{1,i}}{N} \leq a_i^{[n]} \log(1 + \rho_i) + b_i^{[n]}, \quad (34a)$$

$$\begin{aligned} \log(t_{1,i}^{[n]}) + \frac{t_{1,i} - t_{1,i}^{[n]}}{t_{1,i}^{[n]}} + 2\log(1 + \rho_i^{[n]}) + \frac{2(\rho_i - \rho_i^{[n]})}{1 + \rho_i^{[n]}} \\ \leq \log(t_i). \end{aligned} \quad (34b)$$

To handle the non-convex (27c) and (27d), we rewrite them in their Difference-of-Convex forms, which are given by

$$P_{1,2}|h_1|^2 + P_2|h_2|^2 + \sigma_n^2 - \frac{P_{1,1}|h_1|^2}{\rho_a} \leq 0, \quad (35a)$$

$$P_{1,2}|h_1|^2 + \sigma_n^2 - \frac{P_2|h_2|^2}{\rho_b} \leq 0. \quad (35b)$$

(35a) and (35b) still have concave parts, i.e., $-\frac{P_{1,1}|h_1|^2}{\rho_a}$ and $-\frac{P_2|h_2|^2}{\rho_b}$, which are rewritten by the first-order Taylor approximations. Specifically, the constraints (35a) and (35b) are respectively approximated around the point $(\mathbf{m}^{[n]}, \boldsymbol{\rho}^{[n]})$ at iteration n by

$$\begin{aligned} P_{1,2}|h_1|^2 + P_2|h_2|^2 + \sigma_n^2 \\ - \frac{P_{1,1}|h_1|^2}{\rho_a^{[n]}} + (\rho_a - \rho_a^{[n]}) \frac{P_{1,1}|h_1|^2}{(\rho_a^{[n]})^2} \leq 0, \end{aligned} \quad (36a)$$

$$P_{1,2}|h_1|^2 + \sigma_n^2 - \frac{P_2|h_2|^2}{\rho_b^{[n]}} + (\rho_b - \rho_b^{[n]}) \frac{P_2|h_2|^2}{(\rho_b^{[n]})^2} \leq 0. \quad (36b)$$

The non-convex subproblem (27) is transformed into a convex Problem (37) based on the aforementioned approximation techniques, which can then be solved via the SCA approach. By approximating a series of convex sub-problems, SCA solves the original problem. At iteration n , we solve the following problem using the best solution $(\mathbf{m}^{[n-1]}, \boldsymbol{\rho}^{[n-1]})$ from the preceding iteration $n - 1$:

$$\min_{\mathbf{m}, \boldsymbol{\rho}} 2\exp(-t_a) + 2\exp(-t_b) + \exp(-t_c) \quad (37a)$$

$$\text{s.t. } (34a), (34b), (35a), (35b)(27e)(17b), (17c).$$

C. Rate-Splitting Task Allocation Factor Optimization

When transmit power \mathbf{m} and the offloading factor $\boldsymbol{\lambda}$ are all fixed, the subproblem with respect to $\boldsymbol{\beta}$ is given by

$$\max_{\boldsymbol{\beta}} 2\exp(-t_a) + 2\exp(-t_b) + \exp(-t_c) \quad (38a)$$

$$\text{s.t. } t_i \leq \frac{N[\log(1 + \rho_i) - \frac{\beta_i \lambda_k M_k}{N}]^2}{2[1 - (1 + \rho_i)^{-2}]}, \quad i \in \{a, b, c\}, \quad k \in \mathcal{K} \quad (38b)$$

(17d).

Remark 3: Notice that in (38b), the subscription $i = \{a, c\}$ corresponds to $k = 1$ and $i = b$ corresponds to $k = 2$ based on the definition of M_i in Sec. III-A. We rewrite constraint (38b) as

$$t_i \leq Nc_i(d_i + e_i\beta_i)^2, \quad (39)$$

where $c_i \triangleq \frac{1}{2[1 - (1 + \rho_i)^{-2}]}$ and $d_i \triangleq \log(1 + \rho_i)$ and $e_i \triangleq -\frac{\lambda_i M_k}{N}$.

Similar to (27b), constraint (39) is not convex, $(e_i\beta_i)^2$ is approximated by its first-order Taylor approximation around the point $(\beta_i^{[n]})$ at iteration n which is given by

$$(e_i\beta_i)^2 \geq (e_i\beta_i^{[n]})^2 + 2(\beta_i - \beta_i^{[n]})(e_i\beta_i^{[n]}) \triangleq \Phi(\beta_i^{[n]}). \quad (40)$$

Thus, constraint (38b) is rewritten into

$$t_i \leq Nc_i \left(d_i^2 + 2d_i e_i \beta_i + \Phi(\beta_i^{[n]}) \right). \quad (41)$$

Therefore, subproblem (38) is transformed into

$$\min_{\boldsymbol{\beta}} 2\exp(-t_a) + 2\exp(-t_b) + \exp(-t_c) \quad (42a)$$

$$\text{s.t. } (41), (17d). \quad (42b)$$

Now, it is easy to verify that all these sub-problems Problem (37) and Problem (42) are convex problems, which can be efficiently solved by standard convex problem solver such as CVX [46].

D. Proposed Algorithm, Convergence and Complexity

According to the above three subproblems, AO is applied to solve Problem (21) by utilizing the SCA-based algorithm. Specifically, the offloading factor $\boldsymbol{\lambda}$, transmit power \mathbf{m} and the task-splitting factor $\boldsymbol{\beta}$ are alternately optimized by solving Problem (37) and (42), respectively. The details of the proposed algorithm are summarised in **Algorithm 1** where τ is the tolerance. Define $\epsilon = 2\exp(-t_a) + 2\exp(-t_b) + \exp(-t_c)$ for convenience, and $\epsilon^{[n]} = 2\exp(-t_a^{[n]}) + 2\exp(-t_b^{[n]}) + \exp(-t_c^{[n]})$. At each iteration of Algorithm 1, the power allocation and task-splitting factor are updated by solving Second Order Cone Programming (SOCP) problems. Each SOCP is solved by using interior-point method with the computational complexity of $\mathcal{O}([X]^{3.5})$, where X is the total number of variables in the corresponding SOCP problem. Although an additional variable $\boldsymbol{\rho}$, \mathbf{t} and t_1 are introduced for approximating convex problems, the main complexity still comes from the power allocation and task-splitting factor optimization. With given task-splitting factor, the number of variables of Problem (37) is given by $X_{\text{power allocation}} =$

Algorithm 1: Proposed SCA-based AO algorithm for solving Problem (21)

Initialise: $n \leftarrow 0$, $\epsilon^{[n]} \leftarrow 0$, and feasible $\mathbf{m}^{[n]}$, $\beta^{[n]}$;
Calculate optimal λ_k^* , $k \in \{1, 2\}$ by Lemma 1.

1 **repeat**

2 $n \leftarrow n + 1$;

3 Find optimal $\mathbf{m}^{[n]}$ by solving Problem (37) for given $\lambda^{[n]}$ and $\beta^{[n-1]}$;

4 Find optimal $\beta^{[n]}$ by solving Problem (42) for given $\lambda^{[n]}$ and $\mathbf{m}^{[n]}$;

5 Update

$\epsilon^{[n]} \leftarrow \epsilon^*$, $\lambda^{[n]} \leftarrow \lambda^*$, $\mathbf{m}^{[n]} \leftarrow \mathbf{m}^*$, $\beta^{[n]} \leftarrow \beta^*$;

6 **until** $|\epsilon^{[n]} - \epsilon^{[n-1]}| \leq \tau$;

$(K + 1)$. Similarly, the number of variables of Problem (42) is given by $X_{\text{task-splitting factor}} = (K + 1)$. The total number of iterations required for the convergence is $\mathcal{O}(\log(\tau^{-1}))$, where τ is the convergence tolerance of Algorithm 1. Therefore, the total computation complexity of Algorithm 1 is $\mathcal{O}((K + 1)^{3.5} \log(\tau^{-1}))$.

Next we demonstrate the convergence of Algorithm 1. Define $g(\mathbf{m}^{[n]}, \beta^{[n]})$ as the objective value at the n^{th} iteration. First, from Problem (37) with a given λ and β in step 3 of Algorithm 1, we know

$$\begin{aligned} g(\mathbf{m}^{[n-1]}, \beta^{[n-1]}) &\stackrel{a}{=} g_{\mathbf{m}}(\mathbf{m}^{[n-1]}, \beta^{[n-1]}) \\ &\stackrel{b}{\leq} g_{\mathbf{m}}(\mathbf{m}^{[n]}, \beta^{[n-1]}) \\ &\stackrel{c}{\leq} g(\mathbf{m}^{[n]}, \beta^{[n-1]}), \end{aligned} \quad (43)$$

where $g_{\mathbf{m}}$ represents the objective value of Problem (37). a holds since the first-order Taylor approximations are tight at the given point $(\mathbf{m}^{[n-1]}, \beta^{[n-1]})$. Since the solution of the approximated Problem (37) at the $n-1^{\text{th}}$ iteration is a feasible point for Problem (37) at the n^{th} iteration, it can be solved successfully. Moreover, the objective function is bounded by the transmit power constraints, then b holds. c is due to the objective value of (37) being the lower bound of (27).

Similarly, from Problem (42) with a given λ and \mathbf{m} in step 4 of Algorithm 1, we know

$$\begin{aligned} g(\mathbf{m}^{[n]}, \beta^{[n-1]}) &\stackrel{a}{=} g_{\beta}(\mathbf{m}^{[n]}, \beta^{[n-1]}) \\ &\stackrel{b}{\leq} g_{\beta}(\mathbf{m}^{[n]}, \beta^{[n]}) \\ &\stackrel{c}{\leq} g(\mathbf{m}^{[n]}, \beta^{[n]}), \end{aligned} \quad (44)$$

where g_{β} represents the objective value of Problem (42). a , b and c hold for the same reasons as we described previously. Thus, we can obtain that

$$g(\mathbf{m}^{[n-1]}, \beta^{[n-1]}) \leq g(\mathbf{m}^{[n]}, \beta^{[n]}), \quad (45)$$

which proves that Algorithm 1 generates a non-decreasing sequence of objective values and it is bounded by the power budget.

Remark 4: The proposed system model and algorithm are designed for a SISO two-user system but can be extended to a general MIMO K -user system. In this extension, the expression for SCP must be revised. Specifically, from (15) and (16), the SCP in the two-user system is given as $P_s = \prod_{k=1}^2 (1 - \epsilon_k)$. By generalizing to a K -user system, the SCP expression becomes $P_s = \prod_{k=1}^K (1 - \epsilon_k)$. In addition, each ϵ_k needs to be re-derived, accounting for the effects of error propagation in a similar way. If extended to multiple-antenna scenarios, precoder design shall be considered at the transmitter side instead of power allocation. The algorithm for an uplink MIMO RSMA system in the FBL regime can be referred to [23].

V. NUMERICAL RESULTS

The performance of a FBL RSMA-aided MEC system with two users is evaluated and compared with conventional transmission schemes in this section. The SCP performance of RSMA-aided MEC is illustrated. Here, the performance of RSMA is compared to NOMA.

- NOMA: This is a special case of RSMA where none of the users split their messages in NOMA. The BS sequentially decodes the user messages based on SIC.

Simulations for the Rayleigh Fading channel with 100 channel realisations are performed. The time budget, T , is 10 ms and the time length of blocklength (in symbol), T_s , is 0.0025 ms. The CPU computation is $C_{\text{cpu}} = 1000$ cycles/bits, $f_{\text{user}} = 0.5$ GHz and L is assumed to be 5. Without loss of generality, it is assumed that the noise variance is 1, $\sigma_n^2 = 1$. The tolerance of the algorithm is set to be $\tau = 10^{-3}$. Here, the decoding orders of $s_{1,1} \rightarrow s_2 \rightarrow s_{1,2}$ of RSMA and $s_1 \rightarrow s_2$ of NOMA are chosen, respectively according to [26].

A. The SCP versus Task Size

The trend of SCP as the size of tasks increases is shown in Fig. 2. Results of four different blocklengths, $N = 250, 500, 750$ and 1000, are compared. In this simulation, the task size of user-1, M_1 , is from 5k bits to 10k bits and the task size of user-2 is $M_2 = 5.5$ k bits. Solid and dash lines represent the transmit Signal to Noise Ratio (SNR) of 10 dB and 15 dB, respectively. Recall that when $\frac{M_k C_{\text{cpu}}}{f_{\text{user}}} \leq T$, $k \in 1, 2$, user- k can complete its tasks locally within the time budget, making offloading unnecessary. For user-1, with $M_1 = 5$ k bits, the local computation time is $\frac{M_1 C_{\text{cpu}}}{f_{\text{user}}} = 10$ ms $\leq T$, so offloading is not required. In contrast, user-2 has a local computation time of $\frac{M_2 C_{\text{cpu}}}{f_{\text{user}}} = 11$ ms $> T$, necessitating offloading to meet the time budget. Consequently, transmission errors occur only during user-2's offloading process when $M_1 = 5$ k bits and $M_2 = 5.5$ k bits. As M_1 increases, longer local computation time is required for user-1, and offloading to the MEC server becomes necessary for user-1. We now summarize the insights from Fig. 2 as follows.

- Fig. 2 firstly illustrates the enhanced SCP performance as SNR increases, comparing the solid line (SNR=10 dB) and the dashed line (SNR=15 dB). For example, in Fig.

2 (a), with a short blocklength of 250, the SCP of both RSMA and NOMA drops to 0 when the task size reaches and goes beyond 5.5k bits given a transmit SNR of 10 dB. This is because the short blocklength results in a significantly high coding rate in FBL, which, however, can be mitigated by an increased SNR. As a verification, in Fig. 2 (a), when the transmit SNR increases to 15 dB, the SCP is approximately 0.2 (not zero as a comparison) for $M_1 = 5.5k$ bits and drops to 0 when $M_1 = 6k$ bits.

- Secondly, Fig. 2 demonstrates the superiority of RSMA over NOMA in the MEC scheme. For example, Fig. 2 (b), with a task size of 6k bits and a transmit SNR of 15 dB, RSMA achieves a significantly higher SCP of approximately 0.8 with a blocklength of 500, as shown in Fig. 2, compared to NOMA, which achieves an SCP of about 0.6. At a SCP of 0.5 and a blocklength of 750, the maximum task sizes for RSMA are approximately 6.1k bits and 7.4k bits, compared to 5.8k bits and 7k bits for NOMA, at transmit SNRs of 10 dB and 15 dB, respectively, as shown in Fig. 2 (c).

The superiority of RSMA over NOMA comes from the higher flexibility in decoding order and in allocating power to each stream. The streams of the second decoded user would have a considerable impact on the first decoded user's SINR since the decoding order strictly limits NOMA. However, the decoding order can be more flexible to balance the SINR while decoding each stream with the help of RSMA by splitting one user, for instance, the decoding order for RSMA is $s_{1,1} \rightarrow s_2 \rightarrow s_{1,2}$. In this approach, the task M_1 for user-1 is split into two parts which are transmitted by $s_{1,1}$ and $s_{1,2}$. The majority of M_1 , along with a significant portion of user-1's transmit power, is allocated to $s_{1,2}$, which is decoded interference-free after s_2 . This strategy significantly reduces the decoding burden on $s_{1,1}$, enabling more efficient interference management compared to NOMA, where the entire task M_1 must contend with interference. By leveraging task splitting and optimizing the power allocation, RSMA achieves better resource utilization and improves the overall system performance.

- Finally, Fig. 2 (a) - Fig. 2 (d) demonstrates an enlarged performance gain of RSMA over NOMA with the increase of blocklength. Especially in Fig. 2 (d), for RSMA, the maximum task size that user-1 can handle is 6.7k bits at a transmit SNR of 10 dB and 8.2k bits at 15 dB. In comparison, for NOMA, the maximum task size is 6.5k bits at 10 dB and 7.8k bits at 15 dB.

Additionally, the offloading time, $t_2 = NT_s$, increases with the blocklength, reducing the available computation time, t_3 . As a result, the user must offload a larger portion of tasks to the MEC server, leading to a higher coding rate. In this scenario, RSMA proves advantageous by splitting a user's tasks, effectively balancing the SINR of each stream and reducing the offloading error probability.

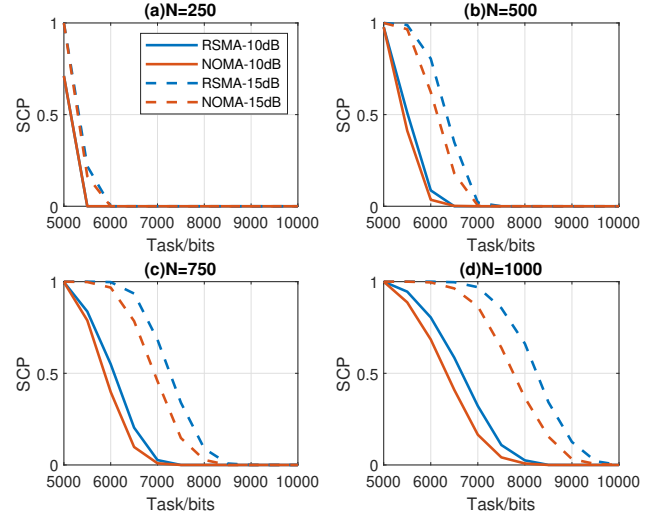


Fig. 2. The successful computation probability performance of RSMA and NOMA versus the size of tasks with two different transmit SNR averaged over 100 random channel realisations. $M_2 = 5.5k$ bits. (a) $N=250$; (b) $N=500$; (c) $N=750$; (d) $N=1000$.

B. The SCP versus Blocklength

Fig. 3 illustrates the relationship between SCP and blocklength. The comparison is made for two task sizes, $M_k = 6k$ bits, $M_k = 7k$ bits and $M_k = 8k$ bits, where $k \in \{1, 2\}$. The transmit SNR is fixed at 15 dB for this simulation. RSMA requires a shorter blocklength than NOMA to achieve the same SCP. For example, when the task size for both users is 6k bits, RSMA achieves an SCP of 0.5 with 50 fewer blocklengths (in symbol) compared to NOMA as indicated by the two solid lines. This demonstrates that RSMA can effectively reduce latency by requiring less blocklength. As the task size increases, the SCP performance gain of RSMA over NOMA becomes more significant, as illustrated by the other two groups of lines. For larger task sizes, the coding rate increases proportionally, placing a heavy burden on decoding s_1 at the MEC server, as its SINR is heavily influenced by s_2 for NOMA. To decode s_2 at a high coding rate, more power is allocated to s_2 , which results in an increasing interference experienced by s_1 .

C. The SCP versus Transmit SNR

Fig. 4 shows the trend of SCP as the transmit SNR increases with more comprehensive simulations. The comparison includes results for five specific blocklengths: $N = 500, 1000, 1500, 2000$ and 3000 . In this simulation, both user-1 (M_1) and user-2 (M_2) have task sizes of 7k bits. The blue lines represent RSMA, while the red lines correspond to NOMA.

In Fig. 4, with blocklength of 500, neither RSMA and NOMA can successfully complete own tasks within the time budget (SCP is 0) since the coding rate is too high. As the blocklength increases, the SCP performance improves with the SCP of NOMA remains consistently lower than RSMA. The gain of RSMA over NOMA does not continue to increase with block-

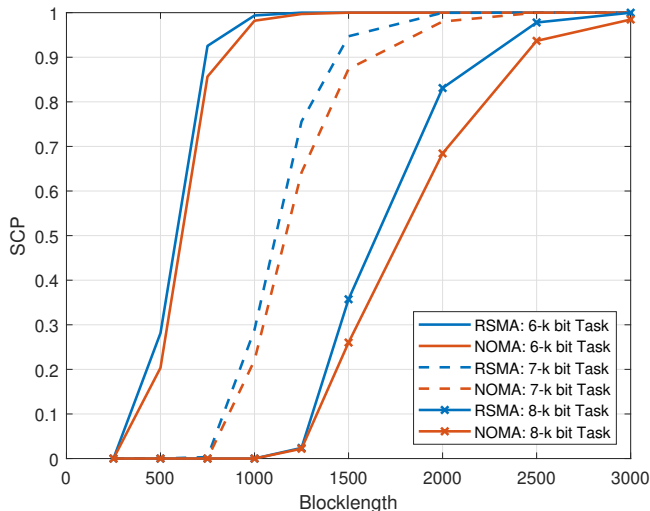


Fig. 3. The successful computation probability performance of RSMA and NOMA versus blocklength with two different task sizes averaged over 100 random channel realisations. Transmit SNR is 15 dB.

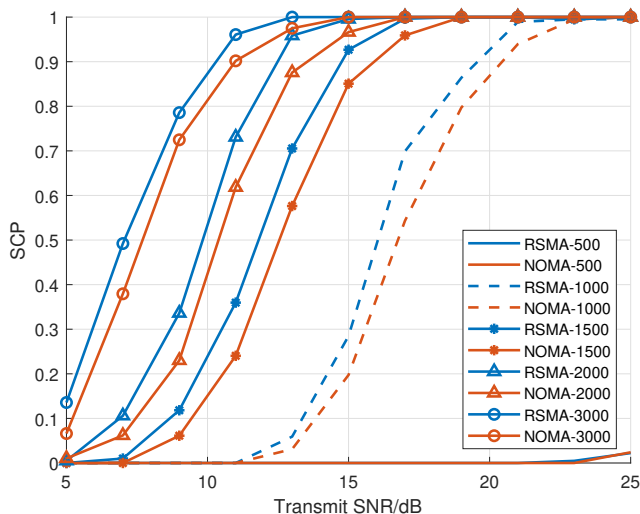


Fig. 4. The successful computation probability performance of RSMA and NOMA versus transmit SNR with four different finite blocklength averaged over 100 random channel realisations. $M_1 = 7k$ bits. $M_2 = 7k$ bits.

length, instead, it saturates at the blocklength of approximately 1000, revealing the performance limit of RSMA.

These numerical results demonstrates that RSMA with a decoding order of $s_{1,1} \rightarrow s_2 \rightarrow s_{1,2}$ achieves a higher SCP compared to NOMA with a decoding order of $s_1 \rightarrow s_2$ in FBL regime. The superior performance of RSMA can be attributed to its ability to allocate transmit power and offloading task size between split streams, balancing the SINR and enhancing overall SCP performance.

VI. CONCLUSION

This paper introduces an RSMA-aided MEC system operating in the FBL regime, where SCP serves as a critical metric. The study focuses on a two-user RSMA-aided MEC system,

aiming to optimize power allocation, task-splitting factor, and offloading factors to maximize SCP. Emphasizing the scenario where only one user's task is split, simulations demonstrate that the RSMA-aided MEC system achieves significantly higher SCP compared to traditional schemes such as NOMA with FBL constraints. Furthermore, RSMA enables reduced latency by achieving comparable SCP to NOMA with shorter blocklengths. These findings shows RSMA-assisted MEC as a promising approach for reliable, low-latency wireless communication systems in the future.

In conclusion, RSMA continuously produces a higher SCP than NOMA in FBL regime, allowing RSMA to provide a more dependable performance. Besides, RSMA achieves much lower latency while achieving the same SCP as NOMA with a shorter blocklength. Since this work is based on a two-user SISO system, the general K -user MIMO system can be studied in the future.

APPENDIX

It is easy to note that the objective function $2 \exp(-\frac{f^2(\gamma_a, M_a)}{2}) + 2 \exp(-\frac{f^2(\gamma_b, M_b)}{2}) + \exp(-\frac{f^2(\gamma_c, M_c)}{2})$ is clearly monotonically increasing with respect to (w.r.t) $\exp(-\frac{f^2(\gamma_i, M_i)}{2})$, $i \in \{a, b, c\}$, for arbitrary \mathbf{m} and β . To verify the monotone of $\exp(-\frac{f^2(\gamma_i, M_i)}{2})$, $i \in \{a, b, c\}$, we first find the derivative of $f(\gamma_i, M_i)^2$. We take $f(\gamma_1, M_a)^2$ for example. First we rewrite $f(\gamma_1, M_a)$ as

$$f(\gamma_1, M_a) = \frac{\log(1 + \gamma_1) - \frac{\lambda_1 M_1}{N}}{D}, \quad (46)$$

where $D = \sqrt{(1 - (1 + \gamma)^{-2})/N}$. Then the first-order derivative of $f(\gamma_1, M_a)^2$ is

$$\frac{\partial f(\gamma_1, M_a)^2}{\partial \lambda_1} = -\frac{2M_1}{DN}(\log(1 + \gamma_1) - \frac{\lambda_1 M_1}{N}) \leq 0, \quad (47)$$

since we have $\log(1 + \gamma_1) - \frac{\lambda_1 M_1}{N} \geq 0$. As $\exp(-\frac{f^2(\gamma_1, M_a)}{2})$ is monotonically decreasing with $f(\gamma_1, M_a)^2$ and $f(\gamma_1, M_a)^2$ is monotonically decreasing w.r.t λ_1 , then $\exp(-\frac{f^2(\gamma_1, M_a)}{2})$ is monotonically increasing w.r.t λ_1 . The proofs are similar for $\exp(-\frac{f^2(\gamma_2, M_b)}{2})$ and $\exp(-\frac{f^2(\gamma_3, M_c)}{2})$. Therefore, the objective function is also monotonically increasing w.r.t each λ .

REFERENCES

- [1] R. Li, "Network 2030 A Blueprint of Technology, Applications and Market Drivers Towards the Year 2030 and Beyond," tech. rep., International Telecommunication Union (ITU), 2019.
- [2] Z. Zhang, Y. Xiao, Z. Ma, M. Xiao, Z. Ding, X. Lei, G. K. Karagiannidis, and P. Fan, "6G Wireless Networks: Vision, Requirements, Architecture, and Key Technologies," *IEEE Vehicular Technology Magazine*, vol. 14, no. 3, pp. 28–41, 2019.
- [3] Y. Mao, C. You, J. Zhang, K. Huang, and K. B. Letaief, "A Survey on Mobile Edge Computing: The Communication Perspective," *IEEE Communications Surveys & Tutorials*, vol. 19, no. 4, pp. 2322–2358, 2017.
- [4] P. Mach and Z. Becvar, "Mobile Edge Computing: A Survey on Architecture and Computation Offloading," *IEEE Communications Surveys & Tutorials*, vol. 19, no. 3, pp. 1628–1656, 2017.

- [5] N. Abbas, Y. Zhang, A. Taherkordi, and T. Skeie, "Mobile Edge Computing: A Survey," *IEEE Internet of Things Journal*, vol. 5, no. 1, pp. 450–465, 2017.
- [6] ETSI, "Mobile-Edge Computing – Introductory Technical White Paper." https://portal.etsi.org/Portals/0/TBpages/MEC/Docs/Mobile-edge_Computing_-_Introductory_Technical_White_Paper.pdf, Sep. 2014. Accessed at 15/12/2024.
- [7] C. You, K. Huang, H. Chae, and B.-H. Kim, "Energy-Efficient Resource Allocation for Mobile-Edge Computation Offloading," *IEEE Transactions on Wireless Communications*, vol. 16, no. 3, pp. 1397–1411, 2016.
- [8] X. Li, R. Fan, H. Hu, N. Zhang, X. Chen, and A. Meng, "Energy-Efficient Resource Allocation for Mobile Edge Computing with Multiple Relays," *IEEE Internet of Things Journal*, vol. 9, no. 13, pp. 10732–10750, 2021.
- [9] H. Sun, F. Zhou, and R. Q. Hu, "Joint Offloading and Computation Energy Efficiency Maximization in A Mobile Edge Computing System," *IEEE Transactions on Vehicular Technology*, vol. 68, no. 3, pp. 3052–3056, 2019.
- [10] Y. Saito, Y. Kishiyama, A. Benjebbour, T. Nakamura, A. Li, and K. Higuchi, "Non-Orthogonal Multiple Access (NOMA) for Cellular Future Radio Access," in *2013 IEEE 77th vehicular technology conference (VTC Spring)*, pp. 1–5, IEEE, 2013.
- [11] S. R. Islam, N. Avazov, O. A. Dobre, and K.-S. Kwak, "Power-Domain Non-Orthogonal Multiple Access (NOMA) in 5G Systems: Potentials and Challenges," *IEEE Communications Surveys & Tutorials*, vol. 19, no. 2, pp. 721–742, 2016.
- [12] W. U. Khan, F. Jameel, T. Ristaniemi, S. Khan, G. A. S. Sidhu, and J. Liu, "Joint Spectral and Energy Efficiency Optimization for Downlink NOMA Networks," *IEEE Transactions on Cognitive Communications and Networking*, vol. 6, no. 2, pp. 645–656, 2019.
- [13] W. U. Khan, J. Liu, F. Jameel, V. Sharma, R. Jäntti, and Z. Han, "Spectral Efficiency Optimization for Next Generation NOMA-Enabled IoT Networks," *IEEE Transactions on Vehicular Technology*, vol. 69, no. 12, pp. 15284–15297, 2020.
- [14] F. Wang, J. Xu, and Z. Ding, "Multi-Antenna NOMA for Computation Offloading in Multiuser Mobile Edge Computing Systems," *IEEE Transactions on Communications*, vol. 67, no. 3, pp. 2450–2463, 2019.
- [15] Z. Ding, J. Xu, O. A. Dobre, and H. V. Poor, "Joint Power and Time Allocation for NOMA-MEC Offloading," *IEEE Transactions on Vehicular Technology*, vol. 68, no. 6, pp. 6207–6211, 2019.
- [16] J. Zhu, J. Wang, Y. Huang, F. Fang, K. Navaie, and Z. Ding, "Resource Allocation for Hybrid NOMA MEC Offloading," *IEEE Transactions on Wireless Communications*, vol. 19, no. 7, pp. 4964–4977, 2020.
- [17] F. Fang, Y. Xu, Z. Ding, C. Shen, M. Peng, and G. K. Karagiannidis, "Optimal Resource Allocation for Delay Minimization in NOMA-MEC Networks," *IEEE Transactions on Communications*, vol. 68, no. 12, pp. 7867–7881, 2020.
- [18] Z. Ding, D. W. K. Ng, R. Schober, and H. V. Poor, "Delay Minimization for NOMA-MEC Offloading," *IEEE Signal Processing Letters*, vol. 25, no. 12, pp. 1875–1879, 2018.
- [19] Y. Ye, R. Q. Hu, G. Lu, and L. Shi, "Enhance Latency-Constrained Computation in MEC Networks Using Uplink NOMA," *IEEE Transactions on Communications*, vol. 68, no. 4, pp. 2409–2425, 2020.
- [20] Z. Liu, Y. Zhu, Y. Hu, P. Sun, and A. Schmeink, "Reliability-Oriented Design Framework in NOMA-Assisted Mobile Edge Computing," *IEEE Access*, vol. 10, pp. 103598–103609, 2022.
- [21] Y. Mao, O. Dizard, B. Clerckx, R. Schober, P. Popovski, and H. V. Poor, "Rate-Splitting Multiple Access: Fundamentals, Survey, and Future Research Trends," *IEEE Communications Surveys & Tutorials*, vol. 24, no. 4, pp. 2073–2126, 2022.
- [22] Y. Mao, B. Clerckx, and V. O. Li, "Rate-Splitting Multiple Access for Downlink Communication Systems: Bridging, Generalizing, and Outperforming SDMA and NOMA," *Journal on Wireless Communications and Networking*, no. 133 (2018), 2018.
- [23] J. Xu and B. Clerckx, "Max-Min Fairness and PHY-Layer Design of Uplink MIMO Rate-Splitting Multiple Access with Finite Blocklength," *IEEE Transactions on Communications*, pp. 1–1, 2024.
- [24] Y. Xu, Y. Mao, O. Dizard, and B. Clerckx, "Rate-Splitting Multiple Access With Finite Blocklength for Short-Packet and Low-Latency Downlink Communications," *IEEE Transactions on Vehicular Technology*, vol. 71, no. 11, pp. 12333–12337, 2022.
- [25] B. Clerckx, Y. Mao, E. A. Jorswieck, J. Yuan, D. J. Love, E. Erkip, and D. Niyato, "A Primer on Rate-Splitting Multiple Access: Tutorial, Myths, and Frequently Asked Questions," *IEEE Journal on Selected Areas in Communications*, vol. 41, no. 5, pp. 1265–1308, 2023.
- [26] J. Xu, O. Dizard, and B. Clerckx, "Rate-Splitting Multiple Access for Short-Packet Uplink Communications: A Finite Blocklength Analysis," *IEEE Communications Letters*, vol. 27, no. 2, pp. 517–521, 2023.
- [27] Y. Xu, Y. Mao, O. Dizard, and B. Clerckx, "Max-Min Fairness of Rate-Splitting Multiple Access With Finite Blocklength Communications," *IEEE Transactions on Vehicular Technology*, vol. 72, no. 5, pp. 6816–6821, 2023.
- [28] Y. Liu, B. Clerckx, and P. Popovski, "Network Slicing for eMBB, URLLC, and mMTC: An Uplink Rate-Splitting Multiple Access Approach," *IEEE Transactions on Wireless Communications*, 2023.
- [29] M. Diamanti, C. Pelekis, E. E. Tsiropoulou, and S. Papavassiliou, "Delay Minimization for Rate-Splitting Multiple Access-Based Multi-Server MEC Offloading," *IEEE/ACM Transactions on Networking*, vol. 32, no. 2, pp. 1035–1047, 2024.
- [30] F. Xiao, P. Chen, H. Wu, Y. Mao, and H. Liu, "Delay Minimization Using Hybrid RSMA-TDMA for Mobile Edge Computing," *Electronics*, vol. 12, no. 11, p. 2550, 2023.
- [31] P. Chen, H. Liu, Y. Ye, L. Yang, K. J. Kim, and T. A. Tsiftsis, "Rate-Splitting Multiple Access Aided Mobile Edge Computing With Randomly Deployed Users," *IEEE Journal on Selected Areas in Communications*, vol. 41, no. 5, pp. 1549–1565, 2023.
- [32] Y. Hu, M. Serror, K. Wehrle, and J. Gross, "Finite Blocklength Performance of Cooperative Multi-Terminal Wireless Industrial Networks," *IEEE Transactions on Vehicular Technology*, vol. 67, no. 7, pp. 5778–5792, 2018.
- [33] Y. Polyanskiy, H. V. Poor, and S. Verdú, "Channel Coding Rate in the Finite Blocklength Regime," *IEEE Transactions on Information Theory*, vol. 56, no. 5, pp. 2307–2359, 2010.
- [34] W. Yang, G. Caire, G. Durisi, and Y. Polyanskiy, "Optimum Power Control at Finite Blocklength," *IEEE Transactions on Information Theory*, vol. 61, pp. 4598–4615, Sep. 2015.
- [35] G. Ozcan and M. C. Gursoy, "Throughput of Cognitive Radio Systems with Finite Blocklength Codes," *IEEE Journal on Selected Areas in Communications*, vol. 31, no. 11, pp. 2541–2554, 2013.
- [36] S. Xu, T.-H. Chang, S.-C. Lin, C. Shen, and G. Zhu, "Energy-Efficient Packet Scheduling with Finite Blocklength Codes: Convexity Analysis and Efficient Algorithms," *IEEE Transactions on Wireless Communications*, vol. 15, no. 8, pp. 5527–5540, 2016.
- [37] Y. Hu, A. Schmeink, and J. Gross, "Blocklength-Limited Performance of Relaying Under Quasi-Static Rayleigh Channels," *IEEE Transactions on Wireless Communications*, vol. 15, no. 7, pp. 4548–4558, 2016.
- [38] W. Yang, G. Durisi, T. Koch, and Y. Polyanskiy, "Quasi-Static Multiple-Antenna Fading Channels at Finite Blocklength," *IEEE Transactions on Information Theory*, vol. 60, no. 7, pp. 4232–4265, 2014.
- [39] J. Scarlett, V. Y. Tan, and G. Durisi, "The Dispersion of Nearest-Neighbor Decoding for Additive Non-Gaussian Channels," *IEEE Transactions on Information Theory*, vol. 63, no. 1, pp. 81–92, 2016.
- [40] S. Schiessl, H. Al-Zubaidy, M. Skoglund, and J. Gross, "Delay Performance of Wireless Communications with Imperfect CSI and Finite-Length Coding," *IEEE Transactions on Communications*, vol. 66, no. 12, pp. 6527–6541, 2018.

- [41] Y. Hu, M. Ozmen, M. C. Gursoy, and A. Schmeink, "Optimal Power Allocation for QoS-Constrained Downlink Multi-User Networks in The Finite Blocklength Regime," *IEEE Transactions on Wireless Communications*, vol. 17, no. 9, pp. 5827–5840, 2018.
- [42] Y. Zhu, Y. Hu, A. Schmeink, and J. Gross, "Energy Minimization of Mobile Edge Computing Networks with HARQ in The Finite Blocklength Regime," *IEEE Transactions on Wireless Communications*, vol. 21, no. 9, pp. 7105–7120, 2022.
- [43] X. Lai, T. Wu, C. Pan, L. Mai, and A. Nallanathan, "Short-Packet Edge Computing Networks With Execution Uncertainty," *IEEE Transactions on Green Communications and Networking*, 2024.
- [44] J. Liu and Q. Zhang, "Offloading Schemes in Mobile Edge Computing for Ultra-Reliable Low Latency Communications," *Ieee Access*, vol. 6, pp. 12825–12837, 2018.
- [45] F. Wang, J. Xu, X. Wang, and S. Cui, "Joint Offloading and Computing Optimization in Wireless Powered Mobile-Edge Computing Systems," *IEEE transactions on wireless communications*, vol. 17, no. 3, pp. 1784–1797, 2017.
- [46] M. Grant, S. Boyd, and Y. Ye, "CVX: Matlab software for disciplined convex programming," 2009.

